Chinese Chemical Letters 33 (2022) 4655–4658

Contents lists available at ScienceDirect

Chinese Chemical Letters

journal homepage: www.elsevier.com/locate/cclet

Amorphous core/shell Ti-doped SnO_2 with synergistically improved N_2 adsorption/activation and electrical conductivity for electrochemical N_2 reduction

Yu Yan[1], Hongjiao Qu[1], Xiaonan Zheng, Kexin Zhao, Xiaoxiao Li, Yuan Yao*, Yang Liu*

School of Chemistry and Chemical Engineering, Harbin Institute of Technology, Harbin 150080, China

ARTICLE INFO

Article history:
Received 30 September 2021
Revised 17 December 2021
Accepted 22 December 2021
Available online 26 December 2021

Keywords:
Nitrogen reduction reaction
Electrocatalysts
Density functional theory
Heteroatom doping
Synergistical effect

ABSTRACT

Electrochemical nitrogen reduction reaction (NRR) has been considered as an appealing and sustainable method to produce ammonia from N_2 under ambient conditions, attracting increasing interest. Limited by low solubility of N_2 in water and high stability of N≡N triple bond, developing NRR electrocatalysts with both strong N_2 adsorption/activation and high electrical conductivity remain challenging. Here, we demonstrate an efficient strategy to develop NRR electrocatalyst with synergistically enhanced N_2 adsorption/activation and electrical conductivity by heteroatom doping. Combining computational and experimental study, the DFT-designed Ti-doped SnO_2 exhibits significantly enhanced NRR performance with ammonia yield rate of 13.09 μg h^{-1} mg^{-1} at −0.2 V *vs.* RHE. Particularly, the Faradaic efficiency reaches up to 42.6%, outperforming most of Sn-based electrocatalysts. The fundamental mechanism for improving NRR performance of SnO_2 by Ti doping is also revealed. Our work highlights a powerful strategy for developing high-activity electrocatalysts for NRR and beyond.

As one of the most important industrial feedstock, ammonia (NH_3) plays a vital role in modern society and has wide applications in chemical fertilizer, textile, pharmaceutics, and related fields [1,2]. Also, it is considered as an efficient carbon-free energy carrier. Nowadays, ammonia production is still heavily dependent on traditional Haber-Bosch process with iron-based catalyst, in which high temperature and pressure are required to meet the harsh reaction conditions, inevitably producing huge amounts of greenhouse gas CO_2 emission. Therefore, it is essential to find out an alternative way for ammonia synthesis under ambient conditions that can remarkably reduce energy consumption and environmental pollution.

The conversion of N_2 to ammonia *via* electrochemical nitrogen reduction reaction (NRR) is a promising and sustainable strategy to produce ammonia under ambient conditions [3,4]. Recently, a number of electrocatalysts for NRR have been developed, including metal-free materials [5,6], noble metal-based materials [7,8], and transition metal-based materials [9–13]. However, the efficiency and space-time yield of NRR is still limited due to the low solubility in water and high bond energy of N≡N triple bond [14]. To this end, the potential electrocatalysts should enrich active sites to stably adsorb N_2 molecule and efficiently activate inert N≡N triple bond [11,12]. Providing abundant active sites is regarded as the potential way to increase the apparent activity of NRR electrocatalysts [15]. Nanostructuring the catalyst, dispersing the catalyst on supports, and constructing single-atom catalyst could be the efficient strategies to achieve this. Then, tuning the intrinsic activity of each active site is the second key point to boost NRR performance of the electrocatalysts [16]. In general, the electronic structure of NRR catalyst significantly determines the intrinsic activity due to the proton-coupled electron transfer between N_2 molecule and the active site during NRR process [17]. Tailoring the electronic structure of a catalyst could directly change the adsorption behavior of N_2 molecule and activate N≡N triple bond to facilitate the conversion from N_2 molecule to ammonia.

Heteroatom doping can tailor the structure of energy band and tune the electron transfer behavior of the semiconductors to overcome the sluggish reaction kinetics, boosting the catalytic activity. Some works demonstrated that the doped heteroatom could act as the catalytic site and redistribute the charge location on the surface of electrocatalyst, enhancing the chemical adsorption for N_2 molecule [18–20]. The generated unsaturated coordination, vacancy and tunable electronic structure could activate the adsorbed N_2 molecule to boost NRR performance [21–25].

As a semiconductor material, SnO_2 has high stability and low hydrogen evolution reaction (HER) activity, being potential cata-

* Corresponding authors.
E-mail addresses: yyuan@hit.edu.cn (Y. Yao), yang.liu@hit.edu.cn (Y. Liu).
[1] These authors contributed equally to this work.

https://doi.org/10.1016/j.cclet.2021.12.054
1001-8417/

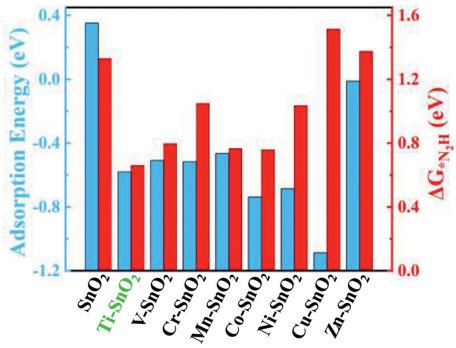

Fig. 1. The calculated N_2 adsorption energies (in blue) and the Gibbs free energy changes of the first hydrogenation step ($\Delta G^*_{N_2H}$, in red) of transition metal-doped SnO_2.

lyst for electrochemical NRR. It suffers from low electrochemical NRR performance owing to poor adsorption for N_2 molecule, limited catalytic sites, and low electrical conductivity [26]. We propose that transition metal doping could boost the NRR performance of SnO_2. Transition metals have diverse d-orbital electronic structures and could promote electron transfer with N_2 molecule via acceptance-donation effect [27]. The strong interactions could decrease the bond order of N_2 molecule and weaken N≡N triple bond, facilitating the adsorption/activation of N_2 molecule. Also, transition metals generally have relatively high electrical conductivity compared to SnO_2, favorable for electron transfer.

Herein, we demonstrated this strategy by doping transition metal into SnO_2 to boost the electrochemical NRR performance. Based on DFT screening, Ti-doped SnO_2 has been proven experimentally to exhibit significantly improved electrochemical NRR performance with yield rate of 13.09 μg h^{-1} mg^{-1} and Faradaic efficiency of 42.6% at −0.2 V *vs.* RHE.

A series of transition metals, including Ti, V, Cr, Mn, Co, Ni, Cu and Zn, were chosen as the heteroatoms to construct transition metal-doped SnO_2 catalysts. To predict their electrochemical NRR activity, DFT calculations were performed to quantitatively evaluate the N_2 adsorption/activation and thermodynamically hydrogenation process. Generally, the adsorption interaction between N_2 molecule and the electrocatalyst should be not too strong or not too weak, simultaneously facilitating the adsorption of N_2 molecule and the desorption of the final product. DFT results showed that N_2 molecule can be stably adsorbed on transition metal atoms with end-on configuration, rather than on Sn or O atoms. As shown in Fig. 1 and Table S1 (Supporting information), one can see that Ti-, V-, Cr- and Mn-doped SnO_2 have much lower adsorption energies than SnO_2, but much higher than others excluding Zn-doped SnO_2, exhibiting the moderate adsorption interaction. Starting from end-on configuration, N_2 molecule could undergo the distal/alternating pathway to successively produce two ammonia molecules *via* continuous hydrogenation steps and the first one to form $^*N_2H$ ($^*N_2 \rightarrow {}^*N_2H$) is generally considered as the potential-determining step (PDS) to determine the NRR activity of catalysts [28,29]. Therefore, we calculated the Gibbs free energy change of this step for SnO_2 and all as-designed electrocatalysts. Among them, Ti-doped SnO_2 has the lowest $\Delta G^*_{N_2H}$ with the value of 0.66 eV in Fig. 1. It is also lower than the previously reported NRR electrocatalysts with high activity, such as MoS_2 with 0.68 eV [30] and Ru single-atom catalyst with 0.73 eV [31]. Therefore, Ti-doped SnO_2 is predicted the potential NRR electrocatalyst that need to be proven by experimental study.

SnO_2 and Ti-doped SnO_2 were synthesized by a facile solvothermal method and no nitrogen-containing raw materials were involved to avoid ammonia contamination as much as possible. As

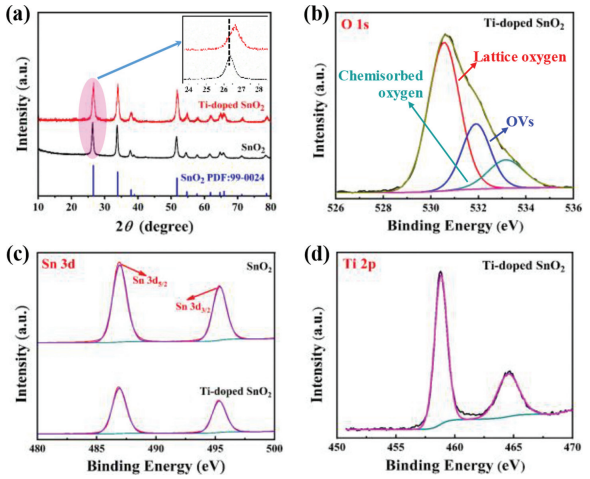

Fig. 2. (a) XRD patterns of SnO_2 and Ti-doped SnO_2 and XPS spectra for (b) O 1s, (c) Sn 3d and (d) Ti 2p.

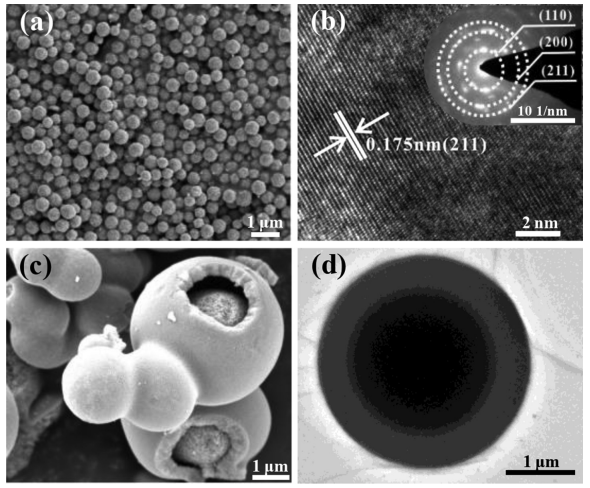

Fig. 3. SEM images and HRTEM images of (a, b) SnO_2 and (c, d) Ti-doped SnO_2.

shown in X-ray diffraction (XRD) patterns in Fig. 2a, one can see that the characteristic diffraction peaks of SnO_2 locate at 26.58°, 33.86° and 51.76°, corresponding to the (110), (101) and (211) planes of SnO_2 (JCPDS No. 99–0024), respectively. The peaks of Ti-doped SnO_2 well correspond to SnO_2 without any impurity or alien phase, showing that Ti is incorporated into SnO_2 [32–34]. The inset exhibits a slight shift of the peak position to high angle, meaning a solid solution with the doped Ti element [35]. The surface chemical states of the as-designed catalysts were characterized to evidence the presence of O, Sn and Ti elements by X-ray photoelectron spectroscopy (XPS) as shown in Figs. 2b–d. The peaks at 458.82 and 464.54 eV in the region of Ti 2p are ascribed to Ti^{4+} [36]. The typical peaks for Sn $3d_{5/2}$ and $3d_{3/2}$ at 486.9 and 495.3 eV indicate that Sn element mainly exists as Sn^{4+} in Ti-doped SnO_2 [37]. The peak positions have ignored shift but the intensities are significantly different in comparison to those in SnO_2 and this could be caused by Ti doping [38]. For the O 1s region, the peaks at 530.43, 531.84 and 533.54 eV are ascribed to lattice oxygen, oxygen atoms in vicinity of the oxygen vacancy and chemisorbed oxygen, respectively [39]. Scanning electron microscopy (SEM) image and the high-resolution transmission electron microscopy (HRTEM) image in Fig. 3 show that SnO_2 has uniform hexagonal nanosphere morphology and (211) crystal plane is exposed with an interplanar distance of 0.175 nm. In comparison, Ti-doped SnO_2 clearly shows an amorphous hollow core/shell

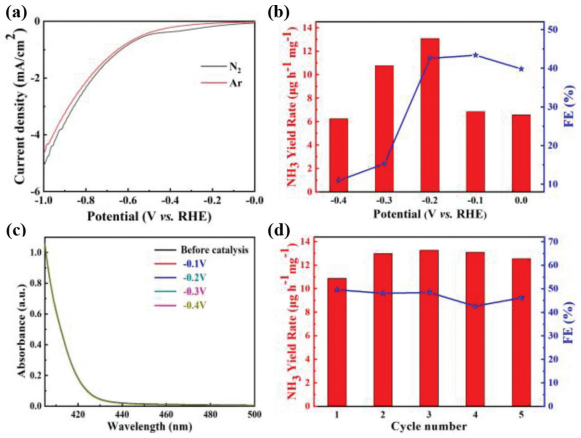

Fig. 4. The electrochemical NRR performance of Ti-doped SnO_2. (a) LSV curves in Ar- and N_2-saturated 0.1 mol/L Na_2SO_4. (b) NH_3 yield rates and Faradaic efficiency at different applied potentials. (c) Chronoamperometry curves for N_2H_4 at different applied potentials. (d) Recycling tests at −0.2 V *vs.* RHE.

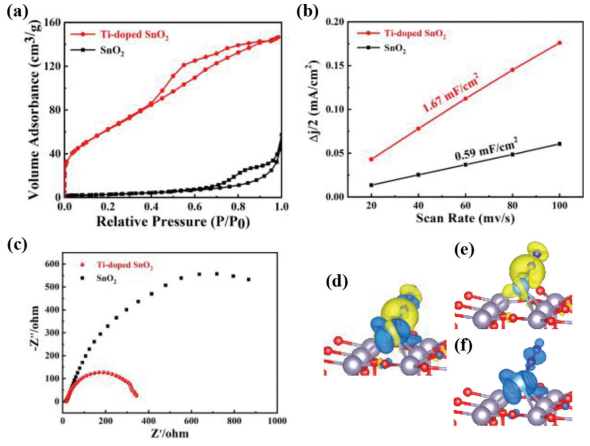

Fig. 5. (a) Nitrogen sorption isotherm, (b) the electrochemical double-layer capacitance analysis at −0.25 V, and (c) EIS analysis of SnO_2 and Ti-doped SnO_2. (d) Difference charge density of N_2 adsorbed on Ti-doped SnO_2 with positive (e) and negative (f) charges represented in yellow and blue, respectively.

structure with holey shell [38,40]. SAED result also supports amorphous structure shown in Fig. S1 (Supporting information). Interestingly, Ti doping remarkably increases the size of SnO_2 particles. This could be caused by the formation of core/shell Ti-doped SnO_2 *via* Ostwald ripening [38].

The standard electrochemical NRR experiments were performed in a two-compartment cell separated by a Nafion 117 membrane in 0.1 mol/L Na_2SO_4 electrolyte under ambient conditions. During the measurement, N_2 gas was continually supplied to the working electrode to react with H^+ from the electrolyte and electron from the electrode react to produce NH_3 on the surface of the working electrode. The produced NH_3 and possible by-product N_2H_4 were quantitatively determined using the indophenol blue method [41] and Watt-Chrisp method [42] with the corresponding calibration curves in Figs. S2 and S3 (Supporting information), respectively. In Fig. 4a, the linear sweep voltammetry (LSV) curves show that Ti-doped SnO_2 has larger current density in N_2-saturated electrolyte than in Ar-saturated condition, corresponding to N_2 response for electrochemical NRR. The ammonia yield rates and Faradaic efficiency of Ti-doped SnO_2 at various electrode potentials on a RHE scale are shown in Fig. 4b with the maximum values of 13.09 μg h^{-1} mg^{-1} and 42.6% at −0.2 V, respectively. The possible by-product N_2H_4 was not detected, exhibiting the excellent selectivity of Ti-doped SnO_2 for converting N_2 to ammonia in Fig. 4c. Also, it shows a prominent cycling stability in 5 cycles shown in Fig. 4d. In comparison, SnO_2 has the ammonia yield rate of 8.23 μg h^{-1} mg^{-1} at −0.8 V with Faradaic efficiency of 5.6% (Fig. S5 in Supporting information) under the similar conditions, consistent with the previous report of cubic sub-micron SnO_2 particles [26]. Evidently, Ti doping can significantly improve the electrochemical NRR performance of SnO_2, being an efficient strategy for developing a high-activity electrocatalyst. Moreover, such excellent NRR performance of Ti-doped SnO_2, particularly for Faradaic efficiency, surpasses most reported Sn-based electrocatalysts for electrochemical NRR under ambient conditions listed in Table S2 (Supporting information) [11,26,31,43–46].

To uncover the origin of the produced NH_3 during electrochemical NRR process, a series of control experiments were constructed [47]. As shown in Fig. S6 (Supporting information), the produced ammonia in each experiment can be reasonably ignored in comparison to that in the standard electrochemical NRR test. This demonstrates that ammonia can only be electrochemically synthesized on the surface of Ti-doped SnO_2 from the supplied N_2 gas. In addition, no nitrogen-containing raw materials were used to synthesize the catalysts mentioned above, implying that the produced ammonia could not be from other nitrogen-containing compounds. In order to exclude the contamination from the environment, the measured ammonia in Ar condition could be subtracted [47]. Therefore, ammonia yield rate was calculated to be 12.35 μg h^{-1} mg^{-1}.

The mechanism of the boosted electrochemical NRR performance of SnO_2 by Ti doping is very informative for understanding the intrinsic catalytic activity of Ti-doped SnO_2 and developing high-activity electrocatalysts for NRR. The good catalysts could have relatively large specific surface area to expose more active sites. The BET results in Fig. 5a exhibit 10 fold increase of the specific surface area of Ti-doped SnO_2 with 230.9 m^2/g compared to SnO_2 with 24.3 m^2/g. It could be caused by the morphology change to generate an amorphous hollow core/shell structure with holey shell due to Ti doping. Furthermore, the electrochemical double-layer capacitance (C_{dl}) measurements in Fig. 5b show that Ti-doped SnO_2 has much bigger electrochemically active surface areas than SnO_2, conducive to the improved electrochemical NRR performance. Faradaic efficiency for NRR is directly related with the electrical conductivity of electrocatalysts. The EIS analysis in Fig. 5c shows that electrical conductivity of SnO_2 is significantly improved by Ti doping, contributing to the markedly increase of FE, supporting the feasibility of our design strategy.

DFT calculations were performed to further investigate the role for Ti doping in improving the catalytic performance of SnO_2. Firstly, Gibbs free energy diagrams of NRR on SnO_2 and Ti-doped SnO_2 (Fig. S7 in Supporting information) were calculated to reveal the thermodynamic behavior in detail. In both distal pathway and alternating pathway, the first dehydrogenation step is determined to be PDS with the biggest energy change, proving the accuracy of our prediction mentioned above. The doping of Ti atom contributes the stability of *NNH intermediate. Secondly, the charge difference density in Figs. 5d–f illustrates that there is electron accumulation and consumption on both Ti atom and N_2 when N_2 is adsorbed on Ti-doped SnO_2. This is a two-way charge transfer between Ti atom and N_2 to achieve acceptance-donation process, favorable for N_2 activation on the catalyst. It is also consistent with the atomic charge variations at each step along the entire distal pathway (Fig. S8 in Supporting information) that both Ti and SnO_2 can accept the electron from the adsorbed N_2 molecule, carrying on the negative charges when N_2 molecule is adsorbed on Ti-doped SnO_2. During the whole NRR process, Ti atom acts as the emissary for electron transport between the adsorbed state $^*N_xH_y$ and SnO_2 substrate.

Thirdly, according to the partial density of states (PDOS) in Fig. S9 (Supporting information), Ti atom has a strong d-π^* orbital coupling with N_2 around the Fermi level. There is an overlap between d-orbital of Ti atom and molecular orbital of the adsorbed N_2 that causes the "push-pull" effect [11], facilitating N_2 activation. This is also in well agreement with the analysis of the charge difference density discussed above.

In summary, we demonstrated a heteroatom doping strategy to synergistically enhance N_2 adsorption/activation and electrical conductivity, boosting the electrochemical NRR activity of semiconductor material. Seven common transition metals were selected as the heteroatom to be doped in SnO_2, as they generally have diverse d-orbital electronic structures and much higher electrical conductivity. Based on DFT prediction on N_2 adsorption and NRR kinetics, Ti-doped SnO_2 was found to be the most potential electrocatalyst for NRR. Then, a facile solvothermal method was used to prepare Ti-doped SnO_2. The obtained Ti-doped SnO_2 exhibits amorphous hollow core/shell structure with holey shell and much higher activity for electrochemical NRR than SnO_2 with ammonia yield rate and Faradaic efficiency of 13.09 μg h^{-1} mg^{-1} and 42.6% at −0.2 V, respectively. Ti doping simultaneously causes multiple effects on SnO_2, including morphology, electrochemical characters, electronic structures, and charge distribution, which facilitate the N_2 adsorption/activation. The improved electrical conductivity promotes the electron transfer during electrochemical hydrogenation process, conducive to Faradaic efficiency.

Declaration of competing interest

The authors declare that they have no known competing financial interests or personal relationships that could have appeared to influence the work reported in this paper.

Acknowledgment

This work was supported by the National Natural Science Foundation of China (No. U2067216). The authors acknowledge Beijng PARATERA Tech Co., Ltd. for providing HPC resources that have contributed to the research results reported within this paper (URL: https://paratera.com/).

Supplementary materials

Supplementary material associated with this article can be found, in the online version, at doi:10.1016/j.cclet.2021.12.054.

References

[1] D. Chanda, R. Xing, T. Xu, et al., Chem. Commun. 57 (2021) 7335–7349.
[2] R. Wang, C. He, W. Chen, C. Zhao, J. Huo, Chin. Chem. Lett. 32 (2021) 3821–3824.
[3] M.M. Shi, D. Bao, B.R. Wulan, et al., Adv. Mater. 29 (2017) 1606550.
[4] M. Wang, S. Liu, T. Qian, et al., Nat. Commun. 10 (2019) 341.
[5] W. Qiu, X.Y. Xie, J. Qiu, et al., Nat. Commun. 9 (2018) 3485.
[6] X. Zhang, T. Wu, H. Wang, et al., ACS Catal. 9 (2019) 4609–4615.
[7] M. Kitano, S. Kanbara, Y. Inoue, et al., Nat. Commun. 6 (2015) 6731.
[8] J. Wang, L. Yu, L. Hu, et al., Nat. Commun. 9 (2018) 1795.
[9] Z. Du, J. Liang, S. Li, et al., J. Mater. Chem. A 9 (2021) 13861–13866.
[10] H. Chen, J. Liang, L. Li, et al., ACS Appl. Mater. Interfaces 13 (2021) 41715–41722.
[11] P. Wang, Y. Ji, Q. Shao, Y. Li, X. Huang, Sci. Bull. 65 (2020) 350–358.
[12] F. He, Z. Wang, S. Wei, J. Zhao, Appl. Surf. Sci. 506 (2020) 144943.
[13] X. Zheng, Y. Liu, Y. Yan, X. Li, Y. Yao, Chin. Chem. Lett. 33 (2022) 1455–1458.
[14] Q. Qin, Y. Zhao, M. Schmallegger, et al., Angew. Chem. Int. Ed. 58 (2019) 13101–13106.
[15] X. Zhu, S. Mou, Q. Peng, et al., J. Mater. Chem. A 8 (2020) 1545–1556.
[16] Y. Yang, M. Luo, W. Zhang, et al., Chem 4 (2018) 2054–2083.
[17] C. Guo, J. Ran, A. Vasileff, S.Z. Qiao, Energy Environ. Sci. 11 (2018) 45–56.
[18] X.W. Lv, Y. Liu, R. Hao, W. Tian, Z.Y. Yuan, ACS Appl. Mater. Interfaces 12 (2020) 17502–17508.
[19] K. Chu, J. Wang, Y.P. Liu, Q.Q. Li, Y.L. Guo, J. Mater. Chem. A 8 (2020) 7117–7124.
[20] Y. Tan, Y. Xu, Z. Ao, Phys. Chem. Chem. Phys. 22 (2020) 13981–13988.
[21] X. Zheng, Y. Liu, Y. Yao, Chem. Eng. J. 426 (2021) 130745.
[22] X. Zheng, Y. Yao, Y. Wang, Y. Liu, Nanoscale 12 (2020) 9696–9707.
[23] D. Jiao, Y. Liu, Q. Cai, J. Zhao, J. Mater. Chem. A 9 (2021) 1240–1251.
[24] X. Liu, H. Zhou, S. Pei, S. Xie, S. You, Chem. Eng. J. 381 (2020) 122740.
[25] H. Li, Z. Zhao, Q. Cai, L. Yin, J. Zhao, J. Mater. Chem. A 8 (2020) 4533–4543.
[26] L. Zhang, X. Ren, Y. Luo, et al., Chem. Commun. 54 (2018) 12966–12969.
[27] M.A. Légaré, G. Bélanger-Chabot, R.D. Dewhurst, et al., Science 359 (2018) 896–900.
[28] J. Deng, J.A. Iñiguez, C. Liu, Joule 2 (2018) 846–856.
[29] X. Cui, C. Tang, Q. Zhang, Adv. Energy Mater. 8 (2018) 1800369.
[30] L. Zhang, X. Ji, X. Ren, et al., Adv. Mater. 30 (2018) 1800191.
[31] Z. Geng, Y. Liu, X. Kong, et al., Adv. Mater. 30 (2018) 1803498.
[32] Y.P. Liu, Y.B. Li, H. Zhang, K. Chu, Inorg. Chem. 58 (2019) 10424–10431.
[33] X. Zhang, X. Huang, D. Liu, et al., Int. J. Hydrog. Energy 43 (2018) 21428–21440.
[34] X. Yang, Y. Ma, Y. Liu, et al., ACS Appl. Mater. Interfaces 13 (2021) 19864–19872.
[35] Z. Lin, C. Guo, Q. Fu, W. Song, Mater. Lett. 102-103 (2013) 47–49.
[36] M. Motola, L. Satrapinskyy, M. Čaplovicová, et al., Appl. Surf. Sci. 434 (2018) 1257–1265.
[37] Y. Shang, W. Shi, R. Zhao, et al., Chin. Chem. Lett. 31 (2020) 2055–2058.
[38] Q. Tian, W. Wei, J. Dai, et al., Appl. Catal. B: Environ. 244 (2019) 45–55.
[39] C. Lv, C. Yan, G. Chen, et al., Angew. Chem. Int. Ed. 57 (2018) 6073–6076.
[40] B. Liu, H.C. Zeng, Small 1 (2005) 566–571.
[41] Y. Zhao, R. Shi, X. Bian, et al., Adv. Sci. 6 (2019) 1802109.
[42] G.W. Watt, J.D. Chrisp, Anal. Chem. 24 (1952) 2006–2008.
[43] X. Chen, Y.T. Liu, C. Ma, J. Yu, B. Ding, J. Mater. Chem. A 7 (2019) 22235–22241.
[44] Y.T. Liu, D. Li, J. Yu, B. Ding, Angew. Chem. Int. Ed. 58 (2019) 16439–16444.
[45] K. Chu, Y.P. Liu, Y.B. Li, J. Wang, H. Zhang, ACS Appl. Mater. Interfaces 11 (2019) 31806–31815.
[46] L. Zhang, M. Cong, X. Ding, et al., Angew. Chem. Int. Ed. 59 (2020) 10888–10893.
[47] C. Chen, Y. Liu, Y. Yao, Eur. J. Inorg. Chem. 2020 (2020) 3236–3241.